LES Analysis of Equivalence Ratio Effect on Turbulent Premixed Characteristics of LPG Flame Front Propagation

Mohamed A. Yehia*, Fawzy Abdel-Aziz, Mohamed M. A. Hassan , Hatem O. Kayed

Department of Mechanical Power, Faculty of Engineering, Cairo University, Cairo, EGYPT

A R T I C L E   I N F O

A B S T R A C T

Turbulent premixed characteristics of LPG are not restricted to change of laminar flame velocity with equivalence ratio. Sudden pressure rise resulting from the ignition of such flammable mixture, peak pressure attained and time required for such peak to be reached should be investigated and tabulated with the same level of attention for loss prevention requirements. The current work is devoted to numerically examine thermodynamic effects of equivalence ratio and the way it would have on overall characteristics of the evolved LPG flame. The model used incorporates Large Eddy Simulation (LES) technique for turbulent reacting flows. The model is validated against available published experimental data. The combustion chamber under study is of 0.00625 m^3 volume with square cross section involving three consecutive baffle-plates and a box to generate high turbulence level. A good numerical representation of experimental initial and boundary conditions resulted in good agreement with experimental data for generated propagating flame and pressure-time history. It was concluded that pressure gradient exists inside the combustion chamber. Peak pressure increases with equivalence ratio until it reaches a maximum at a slightly rich mixture before dropping with further increase of fuel concentration. Same conditions apply to the time required to reach the peak pressure.

1. Introduction

Liquefied Petroleum Gas (LPG) which consists of Propane (C_3H_8) and Butane (C_4H_{10}) as major components is considered to be a reliable energy source among different fossil fuels. LPG is widely spread in engines, domestic stoves and power generation because of its outstanding combustion behavior and low-emission burning characteristics. However, to empower extensive applications of LPG in different uses, thorough investigations and analyses must be performed to understand different topics concerned with its combustion and explosion issues [1]–[7]. Premixed deflagration is considered a type of gas explosion where the flame marches rapidly producing damage and destruction of everything it approaches. The loss caused by overpressure of flame front propagation at explosion instant is worse than the fire itself [8]. Explosions are very complicated to investigate and analyze as result of unsteady interaction between turbulence, chemistry and configuration. At the beginning, they originate as premixed flame deflagration then develop to severe detonation. To diminish the risk accompanying to explosions, overpressures and flame propagation should be properly simulated in the proposed plant. Earlier studies [9] presented

* Corresponding author. Tel.: +201003269999
  E-mail address: myehia@cu.edu.eg.

prediction techniques and methodologies of reducing explosions. Many studies concerning vented explosions devoted to laboratory chambers [4], [5], [10] [11][12], but complexity of fine measurement was challenging issue. Different shapes of laboratory-scale chambers having obstacles were investigated. Walker et al.[13][14] computationally investigated premixed flame propagation and generation of overpressure in a cylindrical vessel containing turbulence-inducing rings. They reported flame location and shape, flow velocities, and overpressure to interpret combustion dynamics inside the vessel. Moen et al. [15] studied the obstacles effect on cylindrical flames spread. They used obstacles formed from spirals of copper with altered pitch that make the flame encounters a sequence of spiral winding obstacles. In stoichiometric methane-air mixtures, obstacle configuration increases flame speed 24 times comparable with no obstacle case. Na'inan et al. [16] investigated the influence of blockage ratio and obstacle pitch on flame propagation and explosion in vented cylindrical vessel. For a low blockage of 30% double obstacle case, they reported separation distance of 1.75 m which generates the most severe explosions at which overpressure approached 3 bar while a flame speed was close to 500 m/s. Dorofeev and Dorofeev et al. [17][18][19] established different mathematical schemes formulating relations between blockage ratio and flame speed. Johansen and Ciccarelli [20]studied the initial stage of promoted flame acceleration in square channel with obstacles and showed its dependence on blockage ratio. At initiation phase of flame acceleration, it was remarked that both boosted turbulence generation and intensive burning rate caused at high blockage ratios enhanced flame acceleration. Yu et al. [21] experimentally studied the effect of various hollow cross-sectional (triangular, square, and circular) obstacles with the same blockage ratio. The maximum explosion characteristics (overpressure, turbulence intensity and flame propagation speed) were achieved for triangular profile. Wen et al. [22]studied the effect of various cross-wise orientations for three obstacle arrangements in vented chamber on deflagration behavior. For the configuration of three centrally located obstacles, deflagration dynamics expressed in flame speed and overpressure achieved the highest values, in which flame velocity speeds up to 82 m/s, whereas the lowest flame velocity is reported at 42 m/s for the configuration with three obstacles mounted on one side of the chamber. Deflagration dynamics are easily reported in experiments for a small-scale configuration but the complexity of conducting fine measurements on a large-scale configuration is challenging issue [4][20].

With the huge advances in computational technology, CFD is considered to be powerful tool and has been used in simulating the explosion in large scale platforms especially in buildings and off-shore processing plants [23]–[25]. CFD predictions could assist engineers and designers in assessment of the optimal configuration and spacing between adjacent buildings in designing structures of processing plants and other facilities. Baraldi et al. [26] adopted (HYMEP) protocol whose goal is to construct model evaluation scheme for CFD in safety assessment simulation that could assist designers of explosion hazards and safety engineering. The protocol scope is to set up standard booklet helping CFD engineers and researchers to evaluate their potentials of efficiently implementing CFD and to assess the precision of CFD schemes as well.

As compared to RANS, large eddy simulation (LES) gainedits reliability as a rigid computational tool that is capable to predict the deflagration characteristics in both small and large-scale platforms. Its strength was revealed for its ability to predict the complicated phenomena of turbulent flows and model unsteady cases like flame instability, extinguishment and ignition.

LES was employed to study phenomenological characteristics of explosions taking place in laboratory vented chamber of a unique obstacle[27];[28]. Di Sarli [29] differentiated between two phenomenological features; obstacle-side combustion and pseudo-confined combustion, that resulted as the polarity between combustion rate and venting rate. Chen et al. investigates using large eddy simulation (LES) with the flame surface density (FSD) model the influence of blockage ratio of an obstructed chamber on the flame propagation and the induced vortex. Appropriate sub-grid-scale (SGS) model is considered to be the essence of perfect application of LES in predicting deflagration dynamics over a broad spectrum of combustion parameters. Its importance is underlined by its contribution to consider the role of chemical reaction rates. Earlier, large volume of studies adopted flamelet approach in different formulations however being restricted to thin wrinkled flame regime [33].

Previous work [34, 35] adopting "dynamic flame surface density" DFSD scheme relying on laminar flamelets have been encouraging in simulating major features of turbulent premixed flames moving in obstructed chambers. Di Sarli et al. [28][29] reported

the significance of applying DFSD scheme as the most adequate SGS model of LES technique in modelling vented explosion of obstructed chambers. Further SGS schemes were used alternatively to flamelets to predict deflagration characteristics in vented explosions[30]–[39].

The literature survey indicates the need to numerically analyze the equivalence ratio effect on the maximum over-pressure attained and the time required to reach the peak pressure in a small scale combustion chamber that is featured by consecutive obstacles to induce further turbulence being filled by different mixtures of LPG-air. The understanding of such effect would greatly benefit safety engineers concerned with handling storage and transport of LPG utilities.

2. THE VENTED COMBUSTION CHAMBER

The vented combustion chamber is that of the University of Sydney, [12]. It is of volume of 0.000625 m^3. The chamber has a square cross-section of 0.05 m and a length of 0.25 m as can be seen in Figure 1. The experimental features for the flame configuration and generated pressure rise have been published in [40] [41] and are taken to the present study in order to perform the model validation. The chamber consists of three built-in exchangeable solid baffle plates to allow for different configurations as shown in Figure 1. This chamber is of special interest because of its small volume and potential to deliver a flame propagating in strong turbulence environment.

The solid baffle plates used are of 0.05 x 0.05 m aluminum frames manufactured from a sheet of thickness of 3mm. Itis made of five 0.004 m wide bars each of 0.005 m wide space separating them, resulting in a blockage ratio of 40%. The plates are at 90 degrees to the solid box in the chamber used in the present study. The baffle plates are denoted B1, B2 and B3 are located at 0.02, 0.05 and 0.08 m above the bottom of the chamber where ignition takes place. The combustion chamber has a built-in solid box of 0.012m in cross-section, which is centrally located 0.096 m above the ignition point extended throughout the chamber cross-section, which causes significant formation to the flow turbulent streamlines. The pressure history is recorded via Piezo-resistive pressure transducers with a range of 0–1bar and a response time of 0.1ms. Two pressure transducers are positioned at top and the bottom of the combustion chamber.
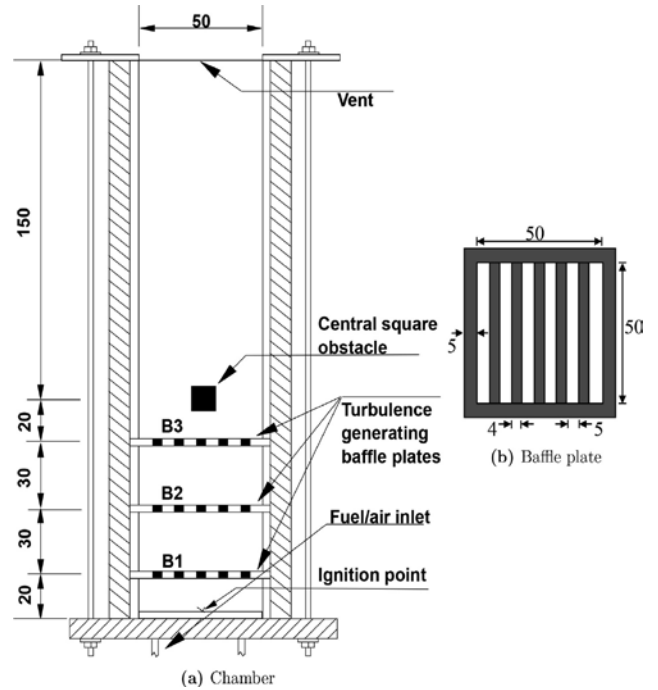

Figure 1: Experimental chamber available for [12]. a) Dimensions of the chamber, three baffle plates; B1, B2 and B3 and the square obstacle, b) Details of the baffle plates, dimensions in mm.

3. THE MATHEMATICAL MODEL

The LES code used here is originally developed by [42]. It solves governing equations of conservation of mass, momentum, energy and the progress variable cwhich takesthe value of zero for the unburned gases andunity for the fully burned products, respectively. Favre filter is used for the governing equations resulting in some unclosed terms which are modeled.

The flow field is spatially filtered; a flow variable $\varphi(x, y, z, t)$ is decomposed of resolved component, $\overline{\varphi}(x, y, z, t)$ and unresolved component, $\dot{\varphi}(x, y, z, t)$. Scales are separated using the filter function G, which is mathematically represented by convolution product as:

$$\overline{\varphi}(x,y,z,t) = \int_v G(x - x', y - y', z - z')\varphi(x,y,z,t)dx'dy'dz'$$

(1)

The function Gused as a filter is related to cut-off length Δ, which is in the range between the Kolomogrov and integral length scales. The filter functions may be taken as the cut-off filter, Gaussian filter and box filter. The box or top hat filter is preferred here due to its simplicity, it is expressed as:

16

$$G(x - x') = \begin{cases} \frac{1}{\bar{\Delta}} & if \ |x - x'| \le \frac{\bar{\Delta}}{2} \\ 0 & otherwise \end{cases} \quad (2)$$

The top hat filter is used and the filtered governing equations in finite volume format are written by the application of box filter width of:

$$\Delta = (\Delta x \Delta y \Delta z)^{1/3} \quad (3)$$

Where $\Delta x, \Delta y$, and Δz are the dimensions of the computational cell. The Favre filtered (mass weighted) equations of continuity, momentum, energy and progress variable are respectively given by:

The Favre-filtered continuity equation:

$$\frac{\partial \bar{\rho}}{\partial t} + \frac{\partial(\bar{\rho}\tilde{u}_j)}{\partial x_j} = 0 \quad (4)$$

The Favre-filtered Navier-Stokes equation:

$$\begin{aligned} \frac{\partial \bar{\rho}\tilde{u}_i}{\partial t} + \frac{\partial(\bar{\rho}\tilde{u}_i\tilde{u}_j)}{\partial x_j} &= -\frac{\partial \bar{P}}{\partial x_i} \\ &+ \frac{\partial}{\partial x_j}\left(2\bar{\mu}\left[\tilde{S}_{ij} - \frac{1}{3}\delta_{ij}\tilde{S}_{kk}\right]\right) \\ &- \frac{\partial \tau_{ij}^{sgs}}{\partial x_j} \end{aligned}$$
$$(5)$$

Where

$$\widetilde{S_{ij}} = \frac{1}{2}\left(\frac{\partial \tilde{u}_i}{\partial x_j} + \frac{\partial \tilde{u}_j}{\partial x_i}\right) \quad (6)$$

τ_{ij}^{sgs} is the residual stresses which represent the effect of the unresolved (Sub-Grid-Scale, SGS) momentum components on the resolved ones. It appears mathematically as a result of the non-linearity of the convective term in the Navier-Stokes equations. In the present work the residual stresses are modeled using the Smagorinsky model [43]based on linear eddy viscosity and it is expressed as:

$$\tau_{ij}^{sgs} - \frac{1}{3}\delta_{ij}\tau_{ij}^{sgs} = -\bar{\mu}_{SGS}(\tilde{S}_{ij} - \frac{1}{3}\delta_{ij}\tilde{S}_{kk}) \quad (7)$$

The SGS eddy viscosity $\bar{\mu}_{SGS}$is expressed as a function of the filter size and the strain rate as:

$$\bar{\mu}_{SGS} = \bar{\rho}C_s\bar{\Delta}^2|\tilde{S}| \quad (8)$$

where $|\tilde{S}| = \sqrt{2\tilde{S}_{ij}\tilde{S}_{ij}}$ and $C_s$is the Smagorinsky model coefficient which is calculated by the dynamic procedure of [44]

The Favre-filtered energy equation is written as:

$$\begin{aligned} \frac{\partial \bar{\rho}\tilde{h}}{\partial t} + \frac{\partial(\bar{\rho}u''_j h'')}{\partial x_j} &= \frac{\partial \bar{P}}{\partial t} + 2\bar{\mu}\left[\tilde{S}_{ij} - \frac{1}{3}\delta_{ij}\tilde{S}_{kk}\right]:\frac{\partial \tilde{u}_j}{\partial x_i} \\ &+ \frac{\partial}{\partial x_j}\left(\frac{\bar{\mu}}{Pr}\frac{\partial \tilde{h}}{\partial x_j}\right) + \bar{\dot{q}}_c \end{aligned}$$
$$(9)$$

The progress variable equation is expressed in the following form:

$$\frac{\partial \bar{\rho}\tilde{c}}{\partial t} + \frac{\partial(\bar{\rho}\tilde{u}_j\tilde{c})}{\partial x_i} + \frac{\partial(\overline{\rho u''_j c''})}{\partial x_j} = \frac{\partial}{\partial x_j}\left(\frac{\bar{\mu}}{S_c}\frac{\partial \tilde{c}}{\partial x_j}\right) + \overline{\dot{\omega}_c} \quad (10)$$

Scalar fluxes in equations (8) and (9) are modeled using a simple gradient transport model as:

$$\bar{\rho}u''_j h'' = \frac{\bar{\mu}_{SGS}}{Pr_t}\frac{\partial \tilde{h}}{\partial x_j} \quad (11)$$

$$\overline{\rho u_j'' c''} = \frac{\bar{\mu}_{SGS}}{Sc_t}\frac{\partial \tilde{c}}{\partial x_j} \quad (12)$$

The rate of the mean chemical reaction is modeled using the laminar flamelet approach [1], expressed as a function of the flame surface density and the mixture laminar burning velocity. The dynamics flame surface density model is used to calculate the sub-grid scale chemical reaction rate.
The flame surface density, which describes the flame surface wrinkling by turbulence, is the flame surface area per unit volume, Σ. The mean chemical reaction rate is assumed to be a function of the FSD as:

$$\overline{\dot{\omega}_c} = R\bar{\Sigma} = \rho_u u_l\bar{\Sigma} \quad (13)$$

Where ρ_u is the density of unburned flow, $u_l$is the laminar burning velocity obtained for LPG from[45], and $\bar{\Sigma}$ is the flame surface density (FSD).
The mean filtered flame surface density is split into resolved and unresolved terms:

$$\bar{\Sigma} = |\overline{\nabla c}| = \prod(\bar{c}, \bar{\Delta}) + f(\bar{c}, \Delta, \prod(\bar{c}, \bar{\Delta})) \quad (14)$$

The unresolved term can be evaluated using the following formulation:

$$\lambda = \bar{\Sigma} - \prod(\bar{c}, \bar{\Delta}) = |\overline{\nabla c}| - \prod(\bar{c}, \bar{\Delta}) \qquad (15)$$

The sub-grid scale contribution of unresolved flame surface density at test filter is assumed to be similar to that at the grid filter and related to each other using Germano identity [3]. Test filter is applied to equation (14). Hence the mean filtered flame surface density is:

$$\hat{\bar{\Sigma}} = |\widehat{\overline{\nabla c}}| = \prod\left(\hat{\bar{c}}, \hat{\bar{\Delta}}\right) + \left[|\widehat{\overline{\nabla c}}| - \prod\left(\hat{\bar{c}}, \hat{\bar{\Delta}}\right)\right] \qquad (16)$$

The second term in the above equation is the unresolved flame surface density at the test filter, which can be expressed as:

$$\Lambda = \left[|\widehat{\overline{\nabla c}}| - \prod\left(\hat{\bar{c}}, \hat{\bar{\Delta}}\right)\right] \qquad (17)$$

The unresolved contributions at test and grid filters are related to each other as follows:

$$\Lambda - \hat{\lambda} = \left[\prod\widehat{(\bar{c}, \bar{\Delta})} - \prod\left(\hat{\bar{c}}, \hat{\bar{\Delta}}\right)\right] \qquad (18)$$

The sub-grid scale flame surface density contribution in the above equation is added to resolved term in equation (16) with the coefficient, C_s. Thus the flame surface density is written:

$$\bar{\Sigma} = \prod(\bar{c}, \bar{\Delta}) + C_s\left[\prod\widehat{(\bar{c}, \bar{\Delta})} - \prod\left(\hat{\bar{c}}, \hat{\bar{\Delta}}\right)\right] \qquad (19)$$

Using equations (17), (18) the unresolved terms in the above equations is:

$$\prod\widehat{(\bar{c}, \bar{\Delta})} = \hat{\bar{\Sigma}}\left(\frac{\bar{\Delta}}{\delta_c}\right)^{D-2} \qquad (20)$$

$$\prod\left(\hat{\bar{c}}, \hat{\bar{\Delta}}\right) = \hat{\bar{\Sigma}}\left(\frac{\hat{\bar{\Delta}}}{\delta_c}\right)^{D-2} \qquad (21)$$

The model coefficient is dynamically deducted by obtaining the sub-grid scale flame surface as a fractal surface [4]. The two equations above are combined and γ is defined as the ratio between the test filter and the grid filter $(\hat{\bar{\Delta}}/\bar{\Delta})$, such that the test filter is greater than the grid filter.

$$C_s = \frac{1}{1-\gamma^{2-D}}\left[\left(\frac{\bar{\Delta}}{\delta_c}\right)^{D-2} - 1\right] \qquad (22)$$

The fractal dimension, D can be calculated using empirical equations [5], [6] or can be dynamically calculated. In the present work, the fractal dimension D is dynamically calculated from:

$$D = 2.0 + \frac{\log\left(\left[\prod\widehat{(\bar{c}, \bar{\Delta})}\right]/\left[\prod\left(\hat{\bar{c}}, \hat{\bar{\Delta}}\right)\right]\right)}{\log(\hat{\bar{\Delta}}/\bar{\Delta})} \qquad (23)$$

4. THE COMPUTATIONAL DOMAIN

A computational domain with initial and boundary conditions is developed. The domain is extended in the direction normal to the outflow boundary so that no pressure reflections get back to the chamber.

The computational domain is superimposed with numerical combustion chamber and obstacles as shown in Figure 2. The combustion chamber has dimensions of 0.050 x 0.050 x 0.250 m. The flame propagates over the baffles and solid obstacle surrounded by solid wall boundary conditions. To ensure that the pressure wave leaves the chamber smoothly, without reflections, the open end of the domain is extended to 0.250 m in the z-direction with a far-field boundary condition. Similarly, the domain is extended to 0.325 m in x and y directions with expansion ratios equal to 1.25 outside the combustion chamber. The 3-dimensional numerical model has been employed with a computational grid of 90×90×336 (2.7 million) cells, (Figure 2). Grid refinement beyond this grid has no significant impact on the results, not shown here.
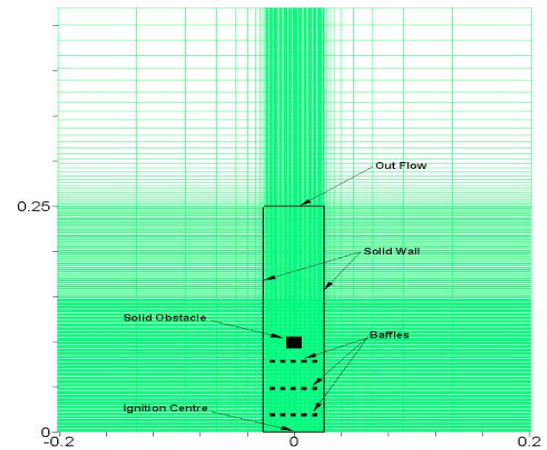

Figure 2: The Computational Domain of the Combustion Chamber

5. RESULTS AND DISCUSSION

Unlike the RANS low resolution due to averaging approach no matter how much fine is the grid, LES analysis results shown in Figures (3-a and 3-b) seem to enable capturing main features defining and

18

controlling the flame front propagation in turbulent environment, namely the wrinkling, stretching and interaction with the eddies, [46]. This, of course is still a far distance away from reality, as the main controlling processes, whether the mass transport with the turbulent eddies or the chemical reaction both take place at a much smaller scale, as the first takes place at the molecular level and the second at the thin fragile flame sheet. Both scales are much thinner than the resolved scales in the LES analysis which are controlled by the cut off ratio which is proportional to the cell dimension. Thus, we are still obtaining modelled values for the main mechanisms. Nevertheless, Figure 3 a and b shows contours of the predicted sub-grid scale application on the flame surface density model for calculating the progress variable at different times and locations. The contours shown are taken to represent the flame propagation. The predicted contours at 9.65, 18.8, 22, 23.3, 24.36, 25.45 and 26 ms are only samples of the detailed results obtained by ANSYS R19 LES analysis. In figure 3.b the iso-lines for the same variable at a range of magnitude from 0.3 to 0.8to follow the thin flame sheet where the chemical reaction is taking place. It is evident that the hemispherical kernel at the bottom of the chamber resulting from the artificial ignition is developed and sustained. The transient propagation of the flame front through the hollow spacing of the baffle plates, the presence of unburned pockets in the vicinity downstream of the three baffles and the higher impact on turbulence generation and thus flame surface area of the obstruction box when compared to that of the box. Compared with LIF-OH images from experiment [41], shown in Figure 4, it can be observed that both the mathematical calculations and experimental images agree in demonstrating the main features of the flame propagation and the increase in turbulence leading to the occurrence of the peak pressure. The predicted images successfully demonstrate a good representation of the high-speed images for the jetting and reconnection of the flame sheets around and downstream from the solid obstacles. On each time the flame impinges obstructions, turbulence level, flame surface area, wrinkling and reaction rate also increase. The peak pressure is reached experimentally at a time of 19.8 ms. This is earlier than the time calculated at around 23 ms as indicated in Figures 3 and 5, as Figure 5 shows a comparison between the experimentally measured and the predicted over-pressure with time. This discrepancy in the time needed to reach the peak pressure is a result of using the present flame surface

density model. A recent parametric study by the present author [47] indicated that this discrepancy can simply be eliminated by varying the initial progress variable set to numerically ignite the mixture inside the chamber.

Figure 6 shows the contours of the calculated pressure gradient inside the combustion chamber at the same time steps indicated previously in Figure 3-a and 3-b for the progress variable. It is shown in the figure that the maximum pressure rise reached is 23 mbar which is almost the same as that indicated experimentally by [41]. The figure demonstrates clearly a pressure gradient that is always highest at the bottom of the chamber and decreases in the upstream direction. This is repeated at each time step, a phenomenon that is not currently confirmed by the experimental data that only provides an average value as obtained from the two piezo-electric pressure transducers mounted at the bottom and the top of the chamber.

The contours of the surface area of the flame are shown in Figure 7. Comparing this figure with the progress variable results shown earlier in Figure 3, we may conclude that both figures map the propagation of the flame front and the effect of obstacles on the increase of the level of turbulence. However, the flame surface area contours also demonstrate the continuous increase of that value as the flame front propagates upwards. It increases from values of 75 m-1 at the first time step shown which is at 9.65 ms until it reaches its maximum of 250 m-1 at time of 24 ms at some downstream locations.

Figure 8 shows the contours for the dimensionless calculates u' normalized by dividing it by the laminar burning velocity ul. Only in the early stage when the flame front just passed the first baffle at the time 9.65 the value is below unity indicating a laminar flame velocity being greater than the turbulent induced u' which then increases to reach 10 times the laminar burning velocity as a result of the repeated obstacles indicating the relatively low importance of the gas characteristics if compared to that of the geometrical configuration in the vicinity of the deflagration process. Figures 9 and 10 show contours of Damkohler number and Reynolds number. The contours indicate a range of 8.0×10^7 to 10^8 and from 150 to 500 for Damkohler and Reynolds respectively. This indicates that the flame front propagation belongs to the thin reaction zone as its combustion regime according to [48], which confirms the validity of the combustion model.

The reasonable results of the validation study for cases of equivalence ratios 0.8 encouraged the

reliance on the model to investigate the effect of increasing the equivalence ratio to 1.23 which correspond to LPG concentration ranging from 3.36 to 5.46% respectively. Though this whole range is falling within the range of the flammability of LPG which is known to be flammable between 1.81 and 8.86%, Figure 11 suggests that the use of a premixed mixture of equivalence of 1.3 does not really result in a significant peak pressure as it just undergoes cyclic pressure rise and fall. As the equivalence ratio increases the peak pressure increases and the time required to reach the peak pressure decreases until the after a value of equivalence ratio of 1.1 when the peak pressure decreases and the time required to reach the peak pressure increases.

Lastly, Figure 12 shows a summation distribution of the LPG laminar burning velocity, peak over-pressure and time required to reach the peak pressure versus the equivalence ratio. This is a preliminary characteristic curve for the deflagration inside the obstacles used in this study. It is assumed that same qualitative features would be universal for other obstruction details and probably to other fuels.

6. CONCLUDING REMARKS

Thermodynamic effects on the performance of LPG-air premixed flame were numerically studied using an LES based mathematical model. The numerical results are validated against available published experimental data obtained from turbulent premixed combustion in a laboratory scale chamber. The CFD model enabled the demonstration of various variables including the progress variable, flame surface density, pressure, Reynolds number, Damkohler number and the rms velocity at different locations and time steps after ignition. It has been shown that a pressure gradient exists inside the combustion chamber. The values obtained for the characteristic parameters confirmed that the flow belongs the thin reaction zone which is adequate for the combustion model used. The numerical modification of the equivalence ratio enabled the mapping of the effect of equivalence ratio on the peak over-pressure and the time required to reach that peak compared to the well documented effect of the equivalence ratio on the laminar burning velocity.
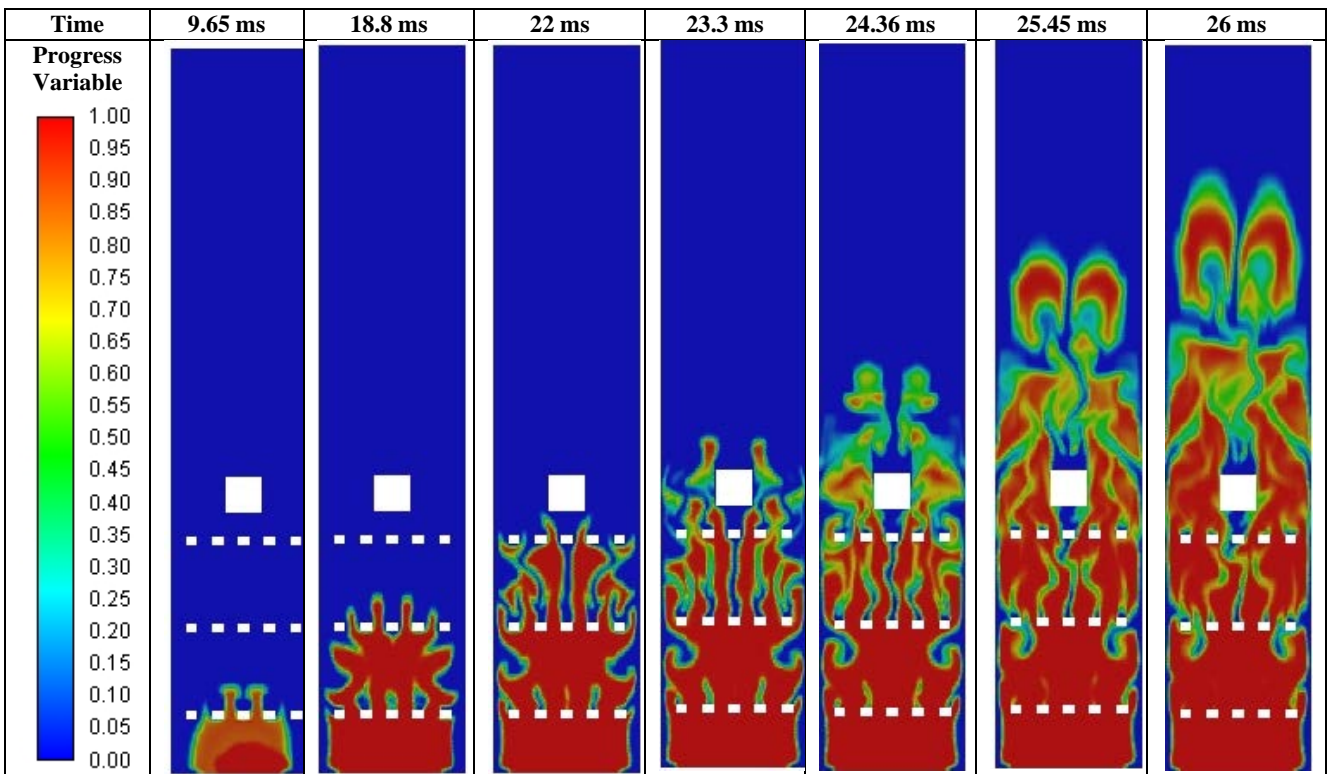

Figure 3a Predicted contours of progress variable at 9.65, 18.8, 22, 23.3, 24.36, 25.45 and 26 ms for a premixed mixture of LPG/air at equivalence ratio of 0.8 as simulated for the BBBS configuration of the Sydney University Combustion Chamber.

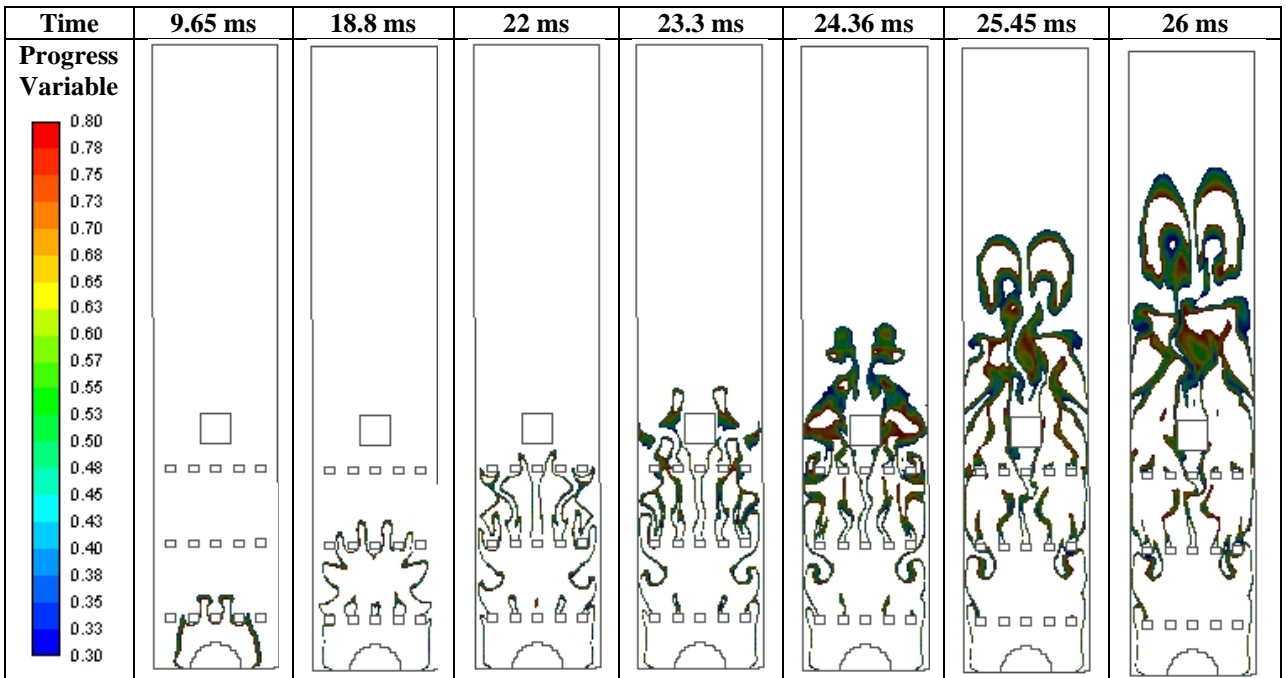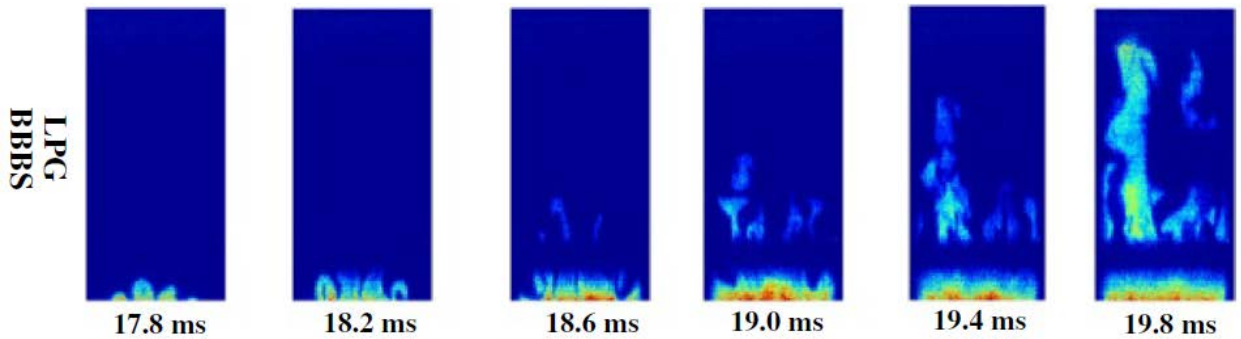| Time	9.65 ms	18.8 ms	22 ms	23.3 ms	24.36 ms	25.45 ms	26 ms

Figure 3b Predicted iso-lines of progress variable at 9.65, 18.8, 22, 23.3, 24.36, 25.45 and 26 ms for a premixed mixture of LPG/air at equivalence ratio of 0.8 as simulated for the BBBS configuration of the Sydney University Combustion Chamber.

Figure 4 LIF OH images of experimentally deflagration of LPG/air mixture on the BBBS configuration as obtained by [41].
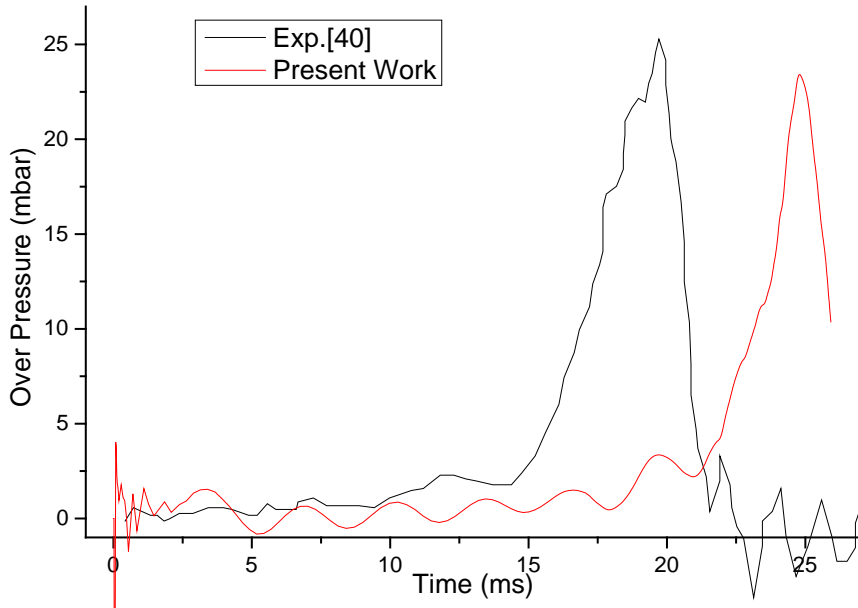
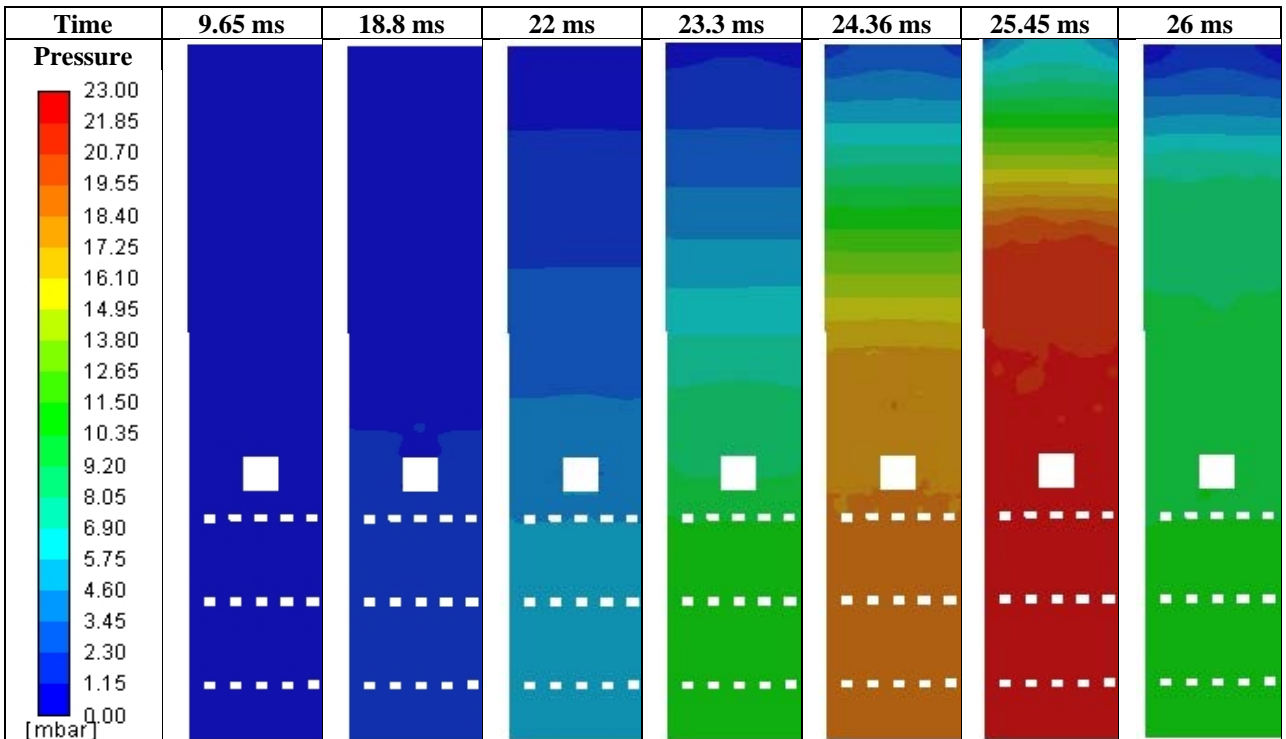Figure 5 Comparison between measured and calculated over-pressure history.

Figure 6 Predicted contours of pressure gradient at 9.65, 18.8, 22, 23.3, 24.36, 25.45 and 26 ms for a premixed mixture of LPG/air at equivalence ratio of 0.8 as simulated for the BBBS configuration of the Sydney University Combustion Chamber.
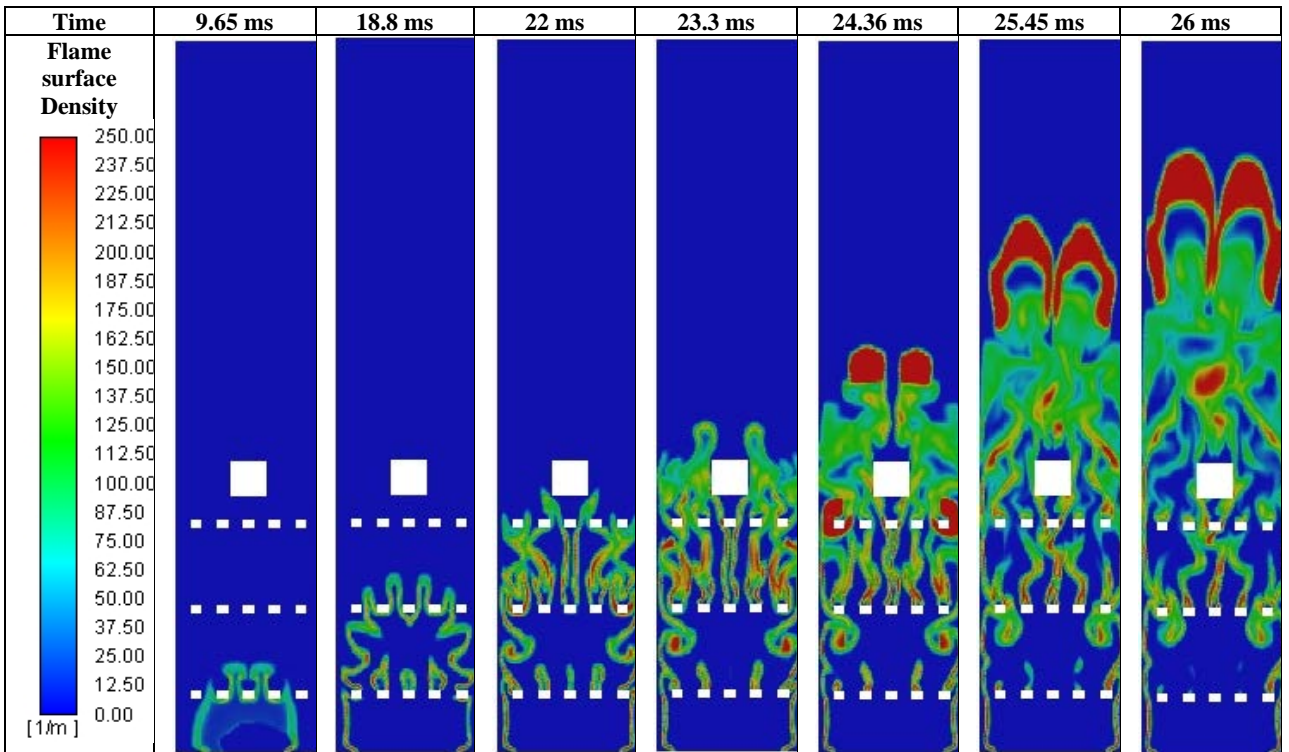
Figure 7 Predicted contours of progress flame surface density at 9.65, 18.8, 22, 23.3, 24.36, 25.45 and 26 ms for a premixed mixture of LPG/air at equivalence ratio of 0.8 as simulated for the BBBS configuration of the Sydney University Combustion Chamber.

Figure 8 Predicted contours of u'/u_l at 9.65, 18.8, 22, 23.3, 24.36, 25.45 and 26 ms for a premixed mixture of LPG/air at equivalence ratio of 0.8 as simulated for the BBBS configuration of the Sydney University Combustion Chamber.
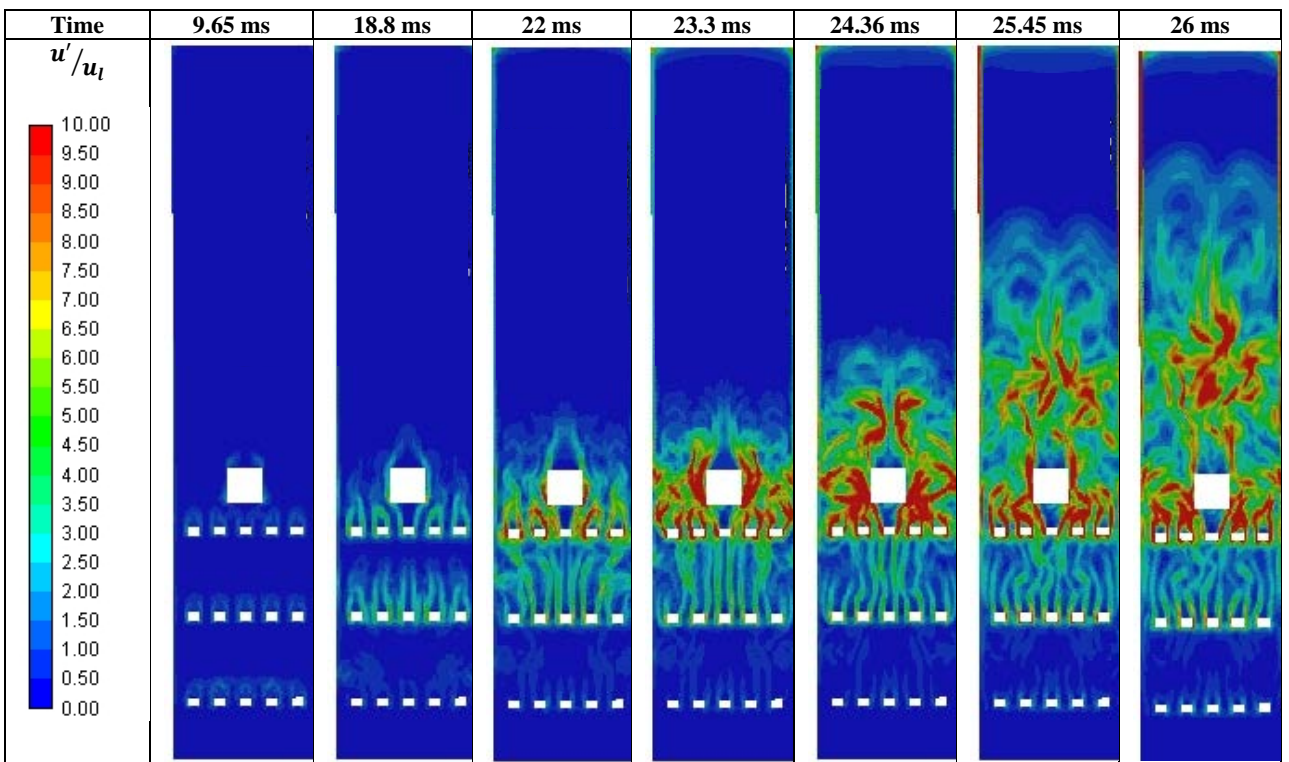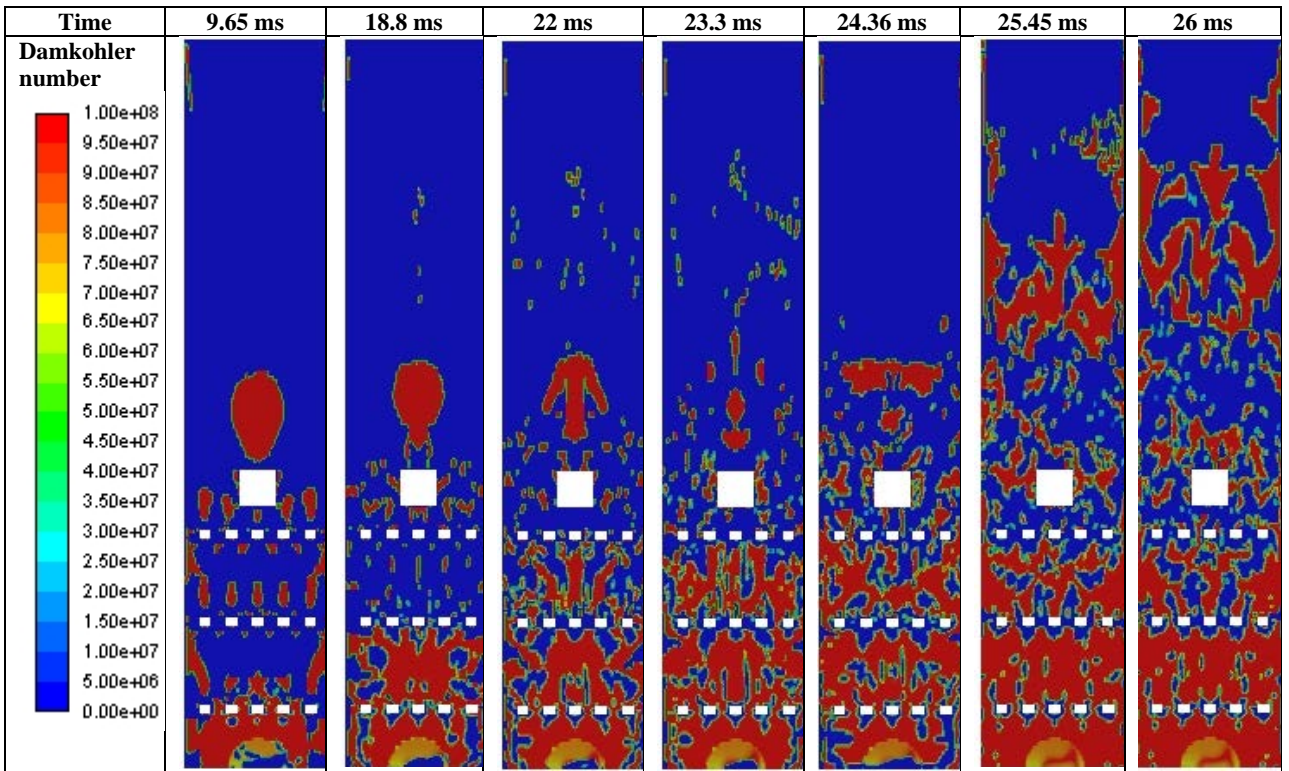
Figure 9 Predicted contours of Damkohler number at 9.65, 18.8, 22, 23.3, 24.36, 25.45 and 26 ms for a premixed mixture of LPG/air at equivalence ratio of 0.8 as simulated for the BBBS configuration of the Sydney University Combustion Chamber.
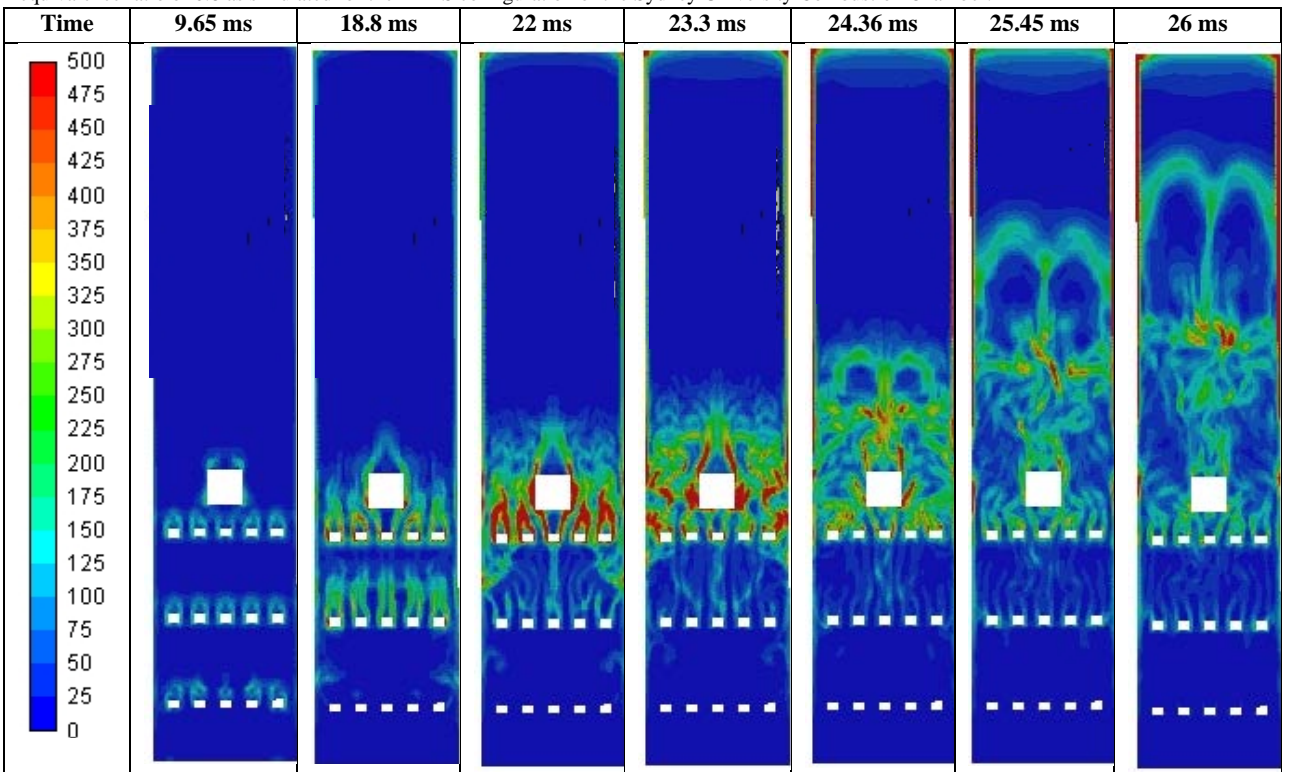

Figure 10 Predicted contours of Reynolds number at 9.65, 18.8, 22, 23.3, 24.36, 25.45 and 26 ms for a premixed mixture of LPG/air at equivalence ratio of 0.8 as simulated for the BBBS configuration of the Sydney University Combustion Chamber.
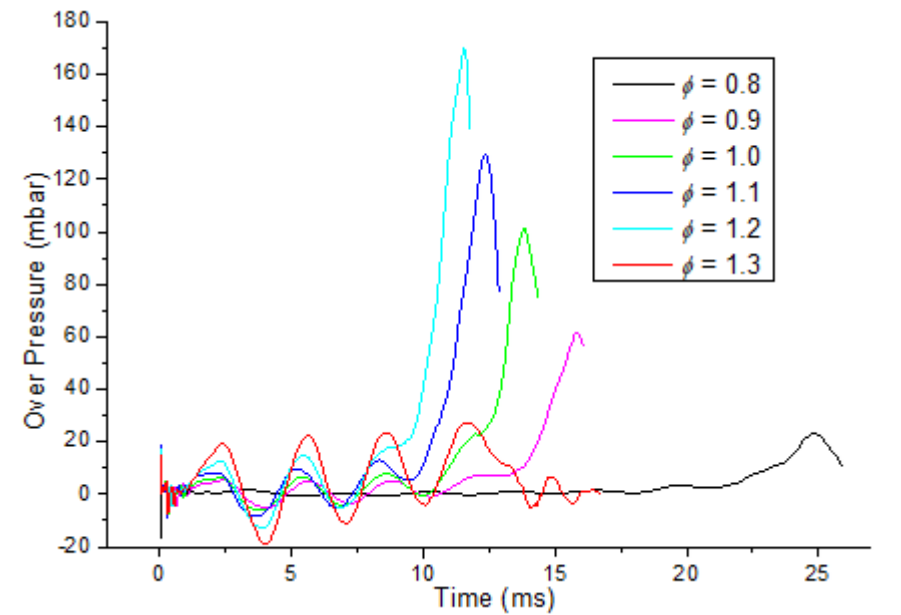
Figure 11 Predicted over-pressure histories for a range of equivalence ratios for LPG/air mixture inside the BBBS combustion chamber.
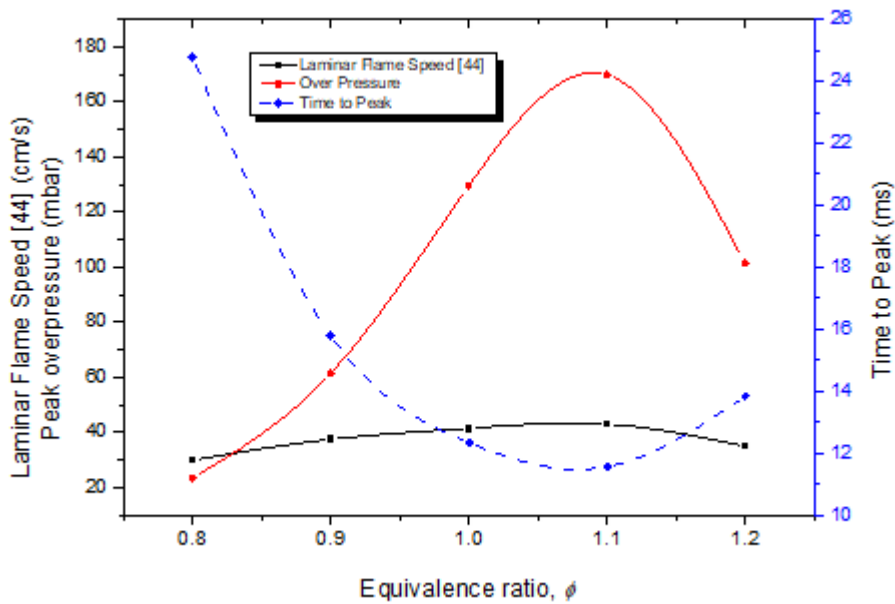

Figure 12 Suggested distribution of Laminar Burning Velocity, Peak Over-Pressure and Time to Peak for LPG/Air Mixtures for Different Equivalence Ratios

Latin Letters

C	Reaction progress variable
D	Mass Diffusivity/ Fractal dimension
G	Convolution function or G field
h	Enthalpy, kJ/kg
L_I	Integral length scale, m
Pr	Prandtl number
Pr_t	Turbulent Prandtl number
p	Pressure, kPa
Q	Heat generation, kJ
q_c	Chemical source term, kJ/kg
R	Mean reaction rate per unit surface area, $kg/s.m^2$
S	Stress tensor, $(m/s)^2$
Sc	Schmidt number
Sc_t	Turbulent Schmidt number
S_{ij}	Strain rate, s^{-1}
T	Temperature, K
T_{ij}	Sub-test-scale stress tensor, $(m/s)^2$
t	Time, s
u	Velocity in x-direction, m/s
u'	RMS fluctuations, m/s

Greek Symbols

λ	Unresolved flame surface density, m^{-1}
μ	Dynamic viscosity, $kg/m.s$
$\bar{\mu}_{SGS}$	SGS turbulent eddy viscosity, m^2/s
$\dot{\omega}_c$	Chemical reaction rate, kg/s
ρ	Fluid density, kg/m^3
ρ_u	Unburned gas density, kg/m^3
δ_{ij}	Kronecker delta
δ_L	Flame thickness, m
δ_c	Lower cut-off scale, m
ϕ	Any fluid property
φ	Equivalence Ratio
τ_{ij}	Residual stress, $(m/s)^2$
$\bar{\Delta}$	Filter width, m
Σ	Flame surface density, m^{-1}
η_k	Kolmogorov scale, m
γ	Ratio of test filter to grid filter
Λ	Unresolved flame surface density at test filter, m^{-1}

References

[1] C. Bae and J. Kim, "Alternative fuels for internal combustion engines," *Proc. Combust. Inst.*, vol. 36, no. 3, pp. 3389–3413, 2017.

[2] N. Gopalaswami, Y. Liu, D. M. Laboureur, B. Zhang, and M. S. Mannan, "Experimental study on propane jet fire hazards: Comparison of main geometrical features with empirical models," *J. Loss Prev. Process Ind.*, vol. 41, pp. 365–375, 2016.

[3] S. Mahesh and D. P. Mishra, "Flame structure of LPG-air Inverse Diffusion Flame in a backstep burner," *Fuel*, vol. 89, no. 8, pp. 2145–2148, 2010.

[4] R. Hall, A. R. Masri, P. Yaroshchyk, and S. S. Ibrahim, "Effects of position and frequency of obstacles on turbulent premixed propagating flames," *Combust. Flame*, 2009.

[5] S. S. Ibrahim and A. R. Masri, "The effects of obstructions on overpressure resulting from premixed flame deflagration," *J. Loss Prev. Process Ind.*, vol. 14, no. 2001, pp. 213–221, 2006.

[6] M. Gerbec *et al.*, "Comparison of UDM and CFD simulations of a time varying release of LPG in geometrical complex environment," *J. Loss Prev. Process Ind.*, vol. 45, pp. 56–68, 2017.

[7] O. Vermorel, P. Quillatre, and T. Poinsot, "LES of explosions in venting chamber : A test case for premixed turbulent combustion models," *Combust. Flame*, vol. 183, pp. 207–223, 2017.

[8] Y. Guo, H. Xiang, Z. Lian, and H. Yuan, "Explosion Properties of LPG—Air Mixtures in a Cylindrical Vessel with Top-Center Ignition," *Chem. Technol. Fuels Oils*, vol. 54, no. 5, pp. 591–598, 2018.

[9] D. Bjerketvedt, J. R. Bakke, and K. Van Wingerden, "Gas Explosion Handbook," vol. 52, no. 96, pp. 1–150, 1997.

[10] A. R. Masri, S. S. Ibrahim, N. Nehzat, and A. R. Green, "Experimental study of premixed flame propagation over various solid obstructions," *Exp. Therm. Fluid Sci.*, 2000.

[11] A. Alharbi, M. Juddoo, and A. R. Masri, "High-Speed LIF-OH Imaging in Premixed Flames Propagating Past Repeated Solid Obstacles," in *18th Australian Fluid Mechanics Conference Launceston, Australia*, 2012, no. December, pp. 9–12.

[12] A. R. Masri, A. Alharbi, S. Meares, and S. S. Ibrahim, "A comparative study of turbulent premixed flames propagating past repeated obstacles," *Ind. Eng. Chem. Res.*, vol. 51, no. 22, pp. 7690–7703, 2012.

[13] M. Fairweather, S. S. Ibrahim, H. Jaggers, and D. G. Walker, "Turbulent premixed flame propagation in a cylindrical vessel," *Symp. Combust.*, vol. 26, no. 1, pp. 365–371, 1996.

[14] M. Fairweather, G. K. Hargrave, S. S. Ibrahim, and D. G. Walker, "Studies of premixed flame propagation in explosion tubes," *Combust. Flame*, vol. 116, no. 4, pp. 504–518, 1999.

[15] I. O. Moen, M. Donato, R. Knystautas, and J. H. Lee, "Flame Acceleration Due to Turbulence Produced by Obstacles *," vol. 32, pp. 21–32.

[16] A. M. Na'inna, H. N. Phylaktou, and G. E. Andrews, "The acceleration of flames in tube explosions with two obstacles as a function of the obstacle separation distance," *J. Loss Prev. Process Ind.*, vol. 26, no. 6, pp. 1597–1603, 2013.

[17] S. B. Dorofeev, "Hydrogen flames in tubes : Critical run-up distances," *Int. J. Hydrogen Energy*, vol. 34, no. 14, pp. 5832–5837, 2009.

[18] S. B. Dorofeev, "Flame acceleration and explosion safety applications," *Proc. Combust. Inst.*, vol. 33, pp. 2161–2175, 2011.

[19] G. Ciccarelli and S. Dorofeev, "Flame acceleration and transition to detonation in ducts," *Prog. Energy Combust. Sci.*, vol. 34, no. 4, pp. 499–550, 2008.

[20] C. T. Johansen and G. Ciccarelli, "Visualization of the unburned gas flow field ahead of an accelerating flame in an obstructed square channel," *Combust. Flame*, vol. 156, no. 2, pp. 405–416, 2009.

[21] M. Yu, K. Zheng, and T. Chu, "Gas explosion flame propagation over various hollow-square obstacles," *J. Nat. Gas Sci. Eng.*, vol. 30, pp. 221–227, 2016.

[22] X. Wen, M. Yu, Z. Liu, G. Li, W. Ji, and M. Xie, "Effects of cross-wise obstacle position on methane-air deflagration characteristics," *J. Loss Prev. Process Ind.*, vol. 26, no. 6, pp. 1335–1340, 2013.

[23] N. R. Popat *et al.*, "Investigations to improve and assess the accuracy of computational fluid dynamic based explosion models," *J. Hazard. Mater.*, vol. 45, no. 1, pp. 1–25, 1996.

[24] B. J. Arntzen, "Modelling of turbulence and combustion for simulation of gas explosions in complex geometries," Norwegian University of Science and Technology, 1998.

[25] L. Sun, H. Yan, S. Liu, and Y. Bai, "Load characteristics in process modules of offshore platforms under jet fire: The numerical study," *J. Loss Prev. Process Ind.*, vol. 47, pp. 29–40, 2017.

[26] D. Baraldi *et al.*, "Development of a model evaluation protocol for CFD analysis of hydrogen safety issues the SUSANA project," *Int. J. Hydrogen Energy*, pp. 1–11, 2016.

[27] S. R. Gubba, S. S. Ibrahim, W. Malalasekera, and A. R. Masri, "LES modeling of premixed deflagrating flames in a small-scale vented explosion chamber with a series of solid obstructions," in *Combustion Science and Technology*, 2008.

[28] V. Di Sarli, A. Di Benedetto, G. Russo, S. Jarvis, E. J. Long, and G. K. Hargrave, "Large eddy simulation and piv measurements of unsteady premixed flames accelerated by obstacles," *Flow, Turbul. Combust.*, vol. 83, no. 2, pp. 227–250, 2009.

[29] V. Di Sarli, A. Di, and G. Russo, "Using Large Eddy Simulation for understanding vented gas explosions in the presence of obstacles," vol. 169, pp. 435–442, 2009.

[30] S. B. Pope, "Small scales, many species and the manifold challenges of turbulent combustion," *Proc. Combust. Inst.*, 2013.

[31] D. H. Rowinski and S. B. Pope, "Computational study of lean premixed turbulent flames using RANSPDF and LESPDF methods," *Combust. Theory Model.*, vol. 17, no. 4, pp. 610–656, 2013.

[32] Y. Yang, H. Wang, S. B. Pope, and J. H. Chen, "Large-eddy simulation / probability density function modeling of a non-premixed CO / H 2 temporally evolving jet flame," *Proc. Combust. Inst.*, vol. 34, no. 1, pp. 1241–1249, 2013.

[33] Y. Ge, M. J. Cleary, and A. Y. Klimenko, "A comparative study of Sandia flame series (D-F) using sparse-Lagrangian MMC modelling," *Proc. Combust. Inst.*, vol. 34, no. 1, pp. 1325–1332, 2013.

[34] K. M. Lyons and W. Wang, "Leading-edge velocities and lifted methane jet flame stability," *J. Combust.*, vol. 2010, 2010.

[35] A. Y. Klimenko and R. W. Bilger, "Conditional moment closure for turbulent combustion," vol. 25, no. 1999, pp. 595–687, 2006.

[36] P. A. Mcmurtry and A. R. Kerstein, "A linear eddy subgrid model for turbulent reacting flows: application to hydrogen-air combustion," *Proc. Combust. Inst.*, vol. 24, pp. 271–278, 1992.

[37] P. Taylor and A. R. Kerstein, "A Linear- Eddy Model of Turbulent Scalar Transport and MixinCombustion Science and Technology g," *Combust. Sci. Technol.*, no. January 2015, pp. 37–41, 2007.

[38] B. A. Sen and S. Menon, "Linear eddy mixing based tabulation and artificial neural networks for large eddy simulations of turbulent flames," *Combust. Flame*, vol. 157, no. 1, pp. 62–74, 2010.

[39] P. Taylor and V. Yakhot, "Propagation Velocity of Premixed Turbulent Flames," *Combust. Sci. Technol.*, no. June 2015, pp. 37–41, 2007.

[40] A. Alharbi, "Turbulent Premixed Flames Propagating Past Repeated Obstacles," , PhD thesis, The University of Sydney, 2013.

[41] A. Alharbi, A. R. Masri, and S. S. Ibrahim, "Turbulent premixed flames of CNG, LPG, and H2propagating past repeated obstacles," *Exp. Therm. Fluid Sci.*, 2014.

[42] M. P. Kirkpatrick, S. W. Armfield, A. R. Masri, and S. S. Ibrahim, "Large Eddy Simulation of a Propagating Turbulent Premixed Flame," *Flow, Turbul. Combust.*, 2003.

[43] S. Smagorinsky, "General circulation experiments with the primitive equations. The basic experiment.," 1963.

[44] M. Germano *et al.*, "A dynamic subgrid - scale eddy viscosity model A dynamic subgrid-scale eddy viscosity model," *Phys. Fluids*, vol. 1760, no. 1991, p. 1760, 2015.

[45] A. S. Huzayyin, H. A. Moneib, M. S. Shehatta, and A. M. A. Attia, "Laminar burning velocity and explosion index of LPG-air and propane-air mixtures," *Fuel*, vol. 87, no. 1, pp. 39–57, 2008.

[46] S. B. Pope, "Flame growth and wrinkling in a turbulent flow," *Appl. Phys. B Lasers Opt.*, vol. 71, no. 5, pp. 711–716, 2000.

[47] M. A. Yehia and M. A. Abdel-Raheem, "Modelling of flammable fuels in small and large scale turbulent environments," *Fuel*, vol. 266, no. January, p. 117110, 2020.

[48] D. Veynante and T. Poinsot, "Quenching processes and premixed turbulent combustion diagrams," *J. Fluid Mech.*, vol. 228, pp. 561–606, 1991.